ХИМИЧЕСКАЯ ФИЗИКА, 2005, том 24, № 9, с. 33–50

ГОРЕНИЕ И ВЗРЫВ

УДК 532.5

STOCHASTIC MODELS FOR THE TURBULENT MIXING OF SCALARS*

© 2005 S. Heinz

University of Wyoming, Department of Mathematics,
1000 East University Avenue, Laramie, WY 82071, USA
E-mail: heinz@uwyo.edu

Received 15.12.2004

The modeling of turbulent reacting flows by stochastic scalar models combined with deterministic velocity models is discussed. First, the improvement of velocity RANS models for compressible wall-bounded turbulent flows is considered. It is shown that an accurate turbulence model can be developed by a stepwise reduction of DNS data. Second, the improvement of scalar PDF models is considered. It is shown that an accurate micromixing model for the turbulent mixing of scalars can be developed on the basis of a projection method. Third, the development of velocity and scalar models for small-scale turbulence is considered. The use of such models represents an alternative to improvements of RANS turbulence and PDF micromixing models since large-scale processes are treated exactly and only small-scale processes are modeled.

1. INTRODUCTION

The use of stochastic models for the calculation of turbulent reacting flows [1–3] is very attractive because chemical reactions can be treated without any need to apply approximations of uncertain generality and accuracy. Such models involve equations for velocities and for scalars (mass fractions of species and temperature). From a computational point of view, it is advantageous to simulate not all the processes involved by stochastic models but to apply hybrid methods. These methods make use of deterministic equations for velocities (Reynolds-Averaged Navier-Stokes (RANS) or Large Eddy Simulation (LES) methods) combined with stochastic equations for scalars (Probability Density Function (PDF) or Filter Density Function (FDF) methods). In this way, the best features of deterministic and stochastic equations are combined: one may apply well-developed modeling and computational methodologies for the calculation of turbulent flow fields where chemical reactions are still treated exactly.

However, currently developed hybrid methods are faced with several problems. The first problem concerns the calculation of flow fields by RANS equations, which are often considered to be relatively inaccurate. A main reason for such shortcomings is the inappropriate use of so-called standard models: essential assumptions in such methods are invalid for many flows. Therefore, there is the question of how it is possible to develop accurate (optimal) RANS models for specific classes of flows (as, *e.g.*, compressible wall-bounded flows, which are relevant to many turbulent combustion problems). Due to the fact that chemical reactions are treated exactly in scalar PDF methods, the performance of turbulent reacting flow calculations depends essentially on the accuracy of scalar mixing models. However, existing micromixing models are characterized by several shortcomings, see below. There is, therefore, the second problem of how previously developed models for scalar mixing can be improved. As an alternative to the improvement of RANS velocity and scalar PDF models, one can try to improve the performance of models by limiting modeling assumptions to small-scale processes, which corresponds to the use of LES and FDF methods. This leads to the third problem that is given by the question of which equations should be used within that approach. These three questions pointed out above will be addressed in sections 2, 3 and 4, respectively. Conclusions of these discussions will be drawn in section 5.

2. VELOCITY RANS EQUATIONS

The first problem pointed out in the introduction will be addressed now on the basis of recently obtained

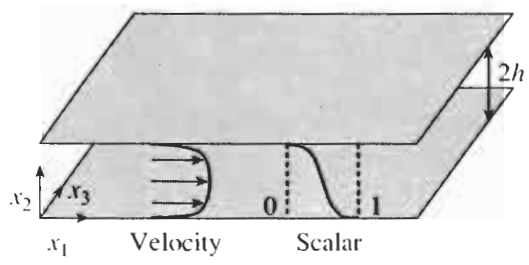

Fig. 1. A sketch of the flow considered. h refers to the half channel height. Mean velocity and scalar profiles appear only in wall-normal direction x_2.

* Данная статья была представлена на Международной конференции по микросмешению в турбулентных реагирующих течениях, 14–17 мая 2004 г., Москва. (The paper was presented at the International conference on micromixing in turbulent reactive flows, May 14–17, 2004, Moscow.)

direct numerical simulation (DNS) data of supersonic channel flow at different Reynolds and Mach numbers [4–6], see the illustration in Fig. 1. The DNS data will be considered first within the frame of a turbulence model, *i.e.*, the turbulence model parameters will be calculated such that the model predictions agree with the corresponding DNS data. These findings can be used then as guideline for the parameterization of turbulence model parameters.

2.1. Direct numerical simulation

The flow dynamics are described by the compressible Navier-Stokes equations for the mass density ρ, velocity U_i (i = 1, 3), temperature T and mass fraction m of a passive scalar,

$$\frac{\partial \rho}{\partial t} + U_k \frac{\partial \rho}{\partial x_k} = -\rho S_{kk}, \tag{2.1a}$$

$$\frac{\partial U_i}{\partial t} + U_k \frac{\partial U_i}{\partial x_k} = \\ = \frac{2}{\rho}\frac{\partial}{\partial x_k}\mu S_{ik}^d - \frac{1}{\rho}\frac{\partial p}{\partial x_i} + \frac{1}{\rho}\left(f + \frac{\partial \langle p \rangle}{\partial x_1}\right)\delta_{i1}, \tag{2.1b}$$

$$\frac{\partial T}{\partial t} + U_k \frac{\partial T}{\partial x_k} = \\ = \frac{1}{\rho}\frac{\partial}{\partial x_k}\frac{\gamma\mu}{\mathrm{Pr}}\frac{\partial T}{\partial x_k} - (\gamma - 1)S_{kk}T + \frac{2}{\rho c_v}\mu S_{ij}^d S_{ji}^d, \tag{2.1c}$$

$$\frac{\partial m}{\partial t} + U_k \frac{\partial m}{\partial x_k} = \frac{1}{\rho}\frac{\partial}{\partial x_k}\frac{\mu}{\mathrm{Sc}}\frac{\partial m}{\partial x_k}. \tag{2.1d}$$

Here, δ_{ij} is the Kronecker delta and the sum convention is applied throughout this paper. The pressure p is given by the thermal equation of state $p = \rho RT$, where R refers to the gas constant. In (2.1b), a force $f = \tau_w/h$ is introduced (τ_w is the wall shear stress and h the half channel height) which replaces the ensemble-averaged pressure gradient $d\langle p \rangle/dx_1$. S_{ik}^d represents the deviatoric part of the rate-of-strain tensor S_{ik}. These quantities are defined by

$$S_{ik}^d = \frac{1}{2}\left(\frac{\partial U_i}{\partial x_k} + \frac{\partial U_k}{\partial x_i} - \frac{2}{3}\frac{\partial U_n}{\partial x_n}\delta_{ik}\right), \\ S_{ik} = \frac{1}{2}\left(\frac{\partial U_i}{\partial x_k} + \frac{\partial U_k}{\partial x_i}\right). \tag{2.2}$$

The closure of (2.1a–d) requires the definition of molecular properties. The expression

$$\mu = \mu_w\left(\frac{T}{T_w}\right)^{0.7} \tag{2.3}$$

is used for the dynamic viscosity, where μ_w and T_w refer to wall values of viscosity and temperature, respectively. The Prandtl number is Pr = 0.7 and the Schmidt number Sc = 1.0. The ratio $\gamma = c_p/c_v$ of specific heats at constant-pressure and constant-volume, respectively, is given by γ = 1.4, and the gas constant $R = c_p - c_v$ is given by R = 287 J/(kg · K). This implies $c_p = \gamma R/(\gamma - 1)$.

The solution of (2.1a–d) was performed by adopting these equations in a pressure-velocity-entropy formulation [7]. A compact 5th-order upwind scheme of Adams and Shariff [8] was used to discretize the hyperbolic (Eulerian) terms. The viscous and heat conduction terms were discretized with a compact 6th-order scheme of Lele [9]. The solution was advanced in time with a third-order "low-storage" Runge-Kutta scheme proposed by Williamson [10]. Equidistant grids were used in (x_1, x_3)-directions. In the wall-normal x_2-direction, points were clustered following tanh-functions [11]. The density-weighted stationary averages considered below (which are referred to by an overbar in contrast to brackets which denote ensemble means) were obtained by averaging over the homogeneous stream- and span wise directions.

2.2. The cases considered

We consider compressible flow of air through a channel of infinitely large plates (with a wall distance of 2h). The flow is driven by a uniform body force. No-slip and impermeability conditions are applied to the velocity field at the walls, and periodic boundary conditions are used in stream- and spanwise directions. Both channel walls are cooled and kept at constant temperature so that there is heat transfer out of the channel allowing supersonic fully-developed flow. A passive scalar is injected at the lower wall and removed at the upper wall [4–6]. The Eqs. (2.1a–d) were solved with these boundary conditions for three sets of the friction Reynolds number Re_τ, bulk Reynolds number Re_0 and Mach number M_0. These parameters are defined by

$$\mathrm{Re}_\tau = \frac{\rho_w u_\tau h}{\mu_w}, \quad \mathrm{Re}_0 = \frac{\rho_0 u_0 h}{\mu_w}, \quad M_0 = \frac{u_0}{a_w}. \tag{2.4}$$

They may be seen as dimensionless measures for the friction velocity, bulk velocity and sound velocity at the wall. These velocities are given by

$$u_\tau = \sqrt{\frac{\tau_w}{\rho_w}}, \quad u_0 = \frac{1}{h}\int_0^h dx_2 \overline{U}_1, \quad a_w = \sqrt{\gamma R T_w}. \tag{2.5}$$

In these expressions, τ_w and ρ_w are the wall shear stress and wall mass density, respectively. ρ_0 is the bulk mass density which is defined in correspondence to u_0. The values for Re_τ, Re_0 and M_0 considered in this way are presented in Table 1, and characteristic simulation data are given in Table 2. The IL data agree well with corresponding DNS data of Moser, Kim and Mansour [12] (which do not involve passive scalar transport), see Foysi *et al.* [6].

As may be seen in Table 1, the cases IL, CL and CH differ by growing Reynolds and Mach numbers Re_τ,

Table 1. **The centerline Reynolds number Re_c centerline Mach number M_c friction Reynolds number Re_τ bulk Reynolds number Re_0 and Mach number M_0 for the cases IL, CL and CH considered**

Case	Re_c	M_c	Re_τ	Re_0	M_0
IL = incompressible and low-Reynolds	3300	0.4	181	2820	0.3
CL = compressible and low-Reynolds	3400	2.2	556	6000	3.0
CH = compressible and high-Reynolds	6100	2.2	1030	11310	3.5

Table 2. **Characteristic simulation data for the IL, CL and CH cases defined in Table 1. N_1, N_2 and N_3 denote the number of grid points in the x_1-, x_2- and x_3-directions, respectively. L_1, L_2 and L_3 are the corresponding domain lengths. Δx_1^+, Δx_2^+ and Δx_3^+ refer to the node distance normalized on the viscous lenght scale $\delta_v = \nu_w/u_\tau$ (regarding Δx_2^+ the minimal and maximal values are given)**

Case	N_1	N_2	N_3	L_1/h	L_2/h	L_3/h	Δx_1^+	$\Delta x_{2\min}^+$	$\Delta x_{2\max}^+$	Δx_3^+
IL	192	129	160	9.6	2	6	9.12	1.02	4.21	6.84
CL	512	221	256	4π	2	$4\pi/3$	13.65	0.89	9.38	8.91
CH	512	301	256	6π	2	$4\pi/3$	37.89	1.27	13.35	16.85

Re_0 and M_0. However, these parameters do not reflect local flow characteristics. This may be seen by considering the local Reynolds number Re and Mach number M,

$$\mathrm{Re} = \frac{\overline{U}_1 h}{\bar{\nu}}, \quad M = \frac{\overline{U}_1}{a}. \tag{2.6}$$

Here, $\overline{U}_1$ is the mean streamwise velocity, $\bar{\nu} = \langle\mu\rangle/\langle\rho\rangle$ is the mean kinematic viscosity, and $a = (\gamma R\overline{T})^{1/2}$ refers to the mean speed of sound. The corresponding curves of Re and M are given in Figs. 2*a*, *b*. This shows that the local Reynolds numbers of IL and CL and the local Mach numbers of CL and CH are basically the same. Hence, the comparison of IL and CL shows the Mach number effect whereas the Reynolds number effect follows from the comparison of CL and CH.

Basic flow characteristics are given in Figs. 2*c*, *d*. The production-to-dissipation ratio P/ε of turbulent kinetic energy k reveals that there is hardly a compressibility effect but a higher Reynolds number has a stronger effect (the plateau region is more pronounced, this means a higher Re implies a larger local-equilibrium region). There is no observable compressibility effect with regard to the normalized inverse dissipation $Sk/\varepsilon = S\tau$ of k ($S = (2\bar{S}_{ik}^d\bar{S}_{ki}^d)^{1/2}$ is the characteristic mean shear rate). The Reynolds number effect is stronger: the dissipation $\varepsilon/(Sk)$ of turbulence increases.

2.3. The turbulence model considered

The DNS data described in the previous section will be considered now within the frame of a turbulence model, *i.e.*, the turbulence model parameters will be calculated such that the model predictions agree with the corresponding DNS data. There are several ways to realize such an analysis. The averaging of the Eqs. (2.1a–d) reveals that one has to provide closures, for example, for the Reynolds stress tensor, turbulent heat and mass flux. Such closures can be obtained on the basis of transport equations of these quantities, or, by the further reduction of these transport equations to algebraic expressions for these quantities. The latter way, which represents the natural first step of such an analysis, will be applied here.

In particular, we consider a k–ω turbulence model. Compared to a k–ε model, this model has the advantage that it can be applied well into the viscous sub-layer, while the k–ω model (with wall functions) requires the first grid point away from the wall to lie in the log layer [3, 13]. By adopting algebraic approximation for turbulent fluxes [1–3, 13], the transport equations for the ensemble-averaged mass density $\langle\rho\rangle$, mass density-weighted velocities, $\overline{U}_i$, temperature $\overline{T}$ and mass fraction $\overline{m}$ read

$$\frac{\partial\langle\rho\rangle}{\partial t} + \overline{U}_k\frac{\partial\langle\rho\rangle}{\partial x_k} = -\langle\rho\rangle\bar{S}_{kk}, \tag{2.7a}$$

$$\frac{\partial\overline{U}_i}{\partial t} + \overline{U}_k\frac{\partial\overline{U}_i}{\partial x_k} = \frac{2}{\langle\rho\rangle}\frac{\partial}{\partial x_k}(\langle\mu\rangle + \mu_T)\bar{S}_{ik}^d - \frac{1}{\langle\rho\rangle}\frac{\partial(\langle p\rangle + 2\langle\rho\rangle k/3)}{\partial x_i} + \frac{1}{\langle\rho\rangle}\left(f + \frac{\partial\langle p\rangle}{\partial x_1}\right)\delta_{i1}, \tag{2.7b}$$

$$\frac{\partial\overline{T}}{\partial t} + \overline{U}_k\frac{\partial\overline{T}}{\partial x_k} = \frac{1}{\langle\rho\rangle}\frac{\partial}{\partial x_k}\gamma\left(\frac{\langle\mu\rangle}{\mathrm{Pr}} + \frac{\mu_T}{\mathrm{Pr}_t}\right)\frac{\partial\overline{T}}{\partial x_k} - (\gamma - 1)\bar{S}_{kk}\overline{T} + \frac{\varepsilon}{c_v} + \frac{1}{c_v}\bar{\nu}S^2, \tag{2.7c}$$

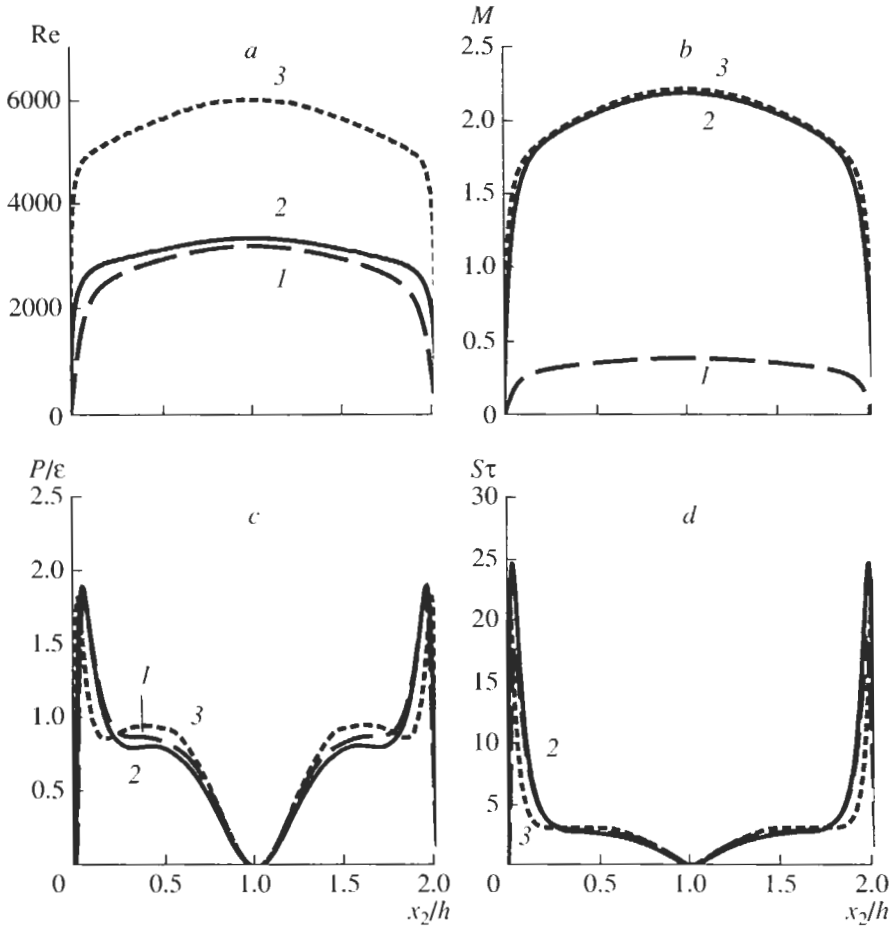

Fig. 2. DNS data for the local Reynolds number Re (*a*), local Mach number M (*b*), production-to-dissipation ratio P/ε of k (*c*) and normalized inverse dissipation (*d*) $Sk/\varepsilon = S\tau$ against the normalized wall-normal coordinate x_2/h (*1* – IL, *2* – CL, *3* – CH).

$$\frac{\partial \bar{m}}{\partial t} + \bar{U}_k \frac{\partial \bar{m}}{\partial x_k} = \frac{1}{\langle \rho \rangle} \frac{\partial}{\partial x_k} \left(\frac{\langle \mu \rangle}{\mathrm{Sc}} + \frac{\mu_T}{\mathrm{Sc}_t} \right) \frac{\partial \bar{m}}{\partial x_k}. \qquad (2.7d)$$

The mean pressure is given by $\langle p \rangle = \langle \rho \rangle R \bar{T}$. Pr_t and Sc_t refer to the turbulence Prandtl and Schmidt numbers, respectively. For the turbulent viscosity μ_T, we apply the parameterization

$$\mu_T = C_\mu \langle \rho \rangle \frac{k}{\omega}. \qquad (2.8)$$

Here, C_μ is a parameter that has to be calculated and $\omega = 1/\tau = \varepsilon/k$ refers to the turbulence frequency. It is assumed that the turbulent kinetic energy k and ω obey the equations

$$\frac{\partial k}{\partial t} + \bar{U}_k \frac{\partial k}{\partial x_k} = \frac{1}{\langle \rho \rangle} \frac{\partial}{\partial x_k} \left(\langle \mu \rangle + \frac{\mu_T}{\mathrm{Pr}_k} \right) \frac{\partial k}{\partial x_k} + C_\mu S^2 \frac{k}{\omega} - k\omega, \qquad (2.9a)$$

$$\frac{\partial \omega}{\partial t} + \bar{U}_k \frac{\partial \omega}{\partial x_k} = \frac{1}{\langle \rho \rangle} \frac{\partial}{\partial x_k} \left(\langle \mu \rangle + \frac{\mu_T}{\mathrm{Pr}_\omega} \right) \frac{\partial \omega}{\partial x_k} - S_\omega \omega^2. \qquad (2.9b)$$

Pr_k and Pr_ω are Prandtl numbers. S_ω refers to the source rate in the turbulence frequency equation, which is usually parameterized by the expression [13]

$$S_\omega = \alpha_2 - \alpha_1 \frac{C_\mu S^2}{\omega^2}; \qquad (2.10)$$

α_1 and α_2 are parameters that have to be calculated. $C_\mu S^2/\omega^2$ represents the modeled production-to-dissipation ratio of turbulent kinetic energy, see (2.9a). Regarding the structure of (2.9a, b) it is worth noting that there is no mean dilatation effect for the flow considered. In correspondence to the negligible influence of dilatational dissipation effects one finds that the contribution of the pressure dilatation $\Pi_d = \overline{(p/\rho)'' S''_{kk}}$ is extremely small: we have $|\Pi_d/(\langle \rho \rangle \varepsilon)| < 0.008$.

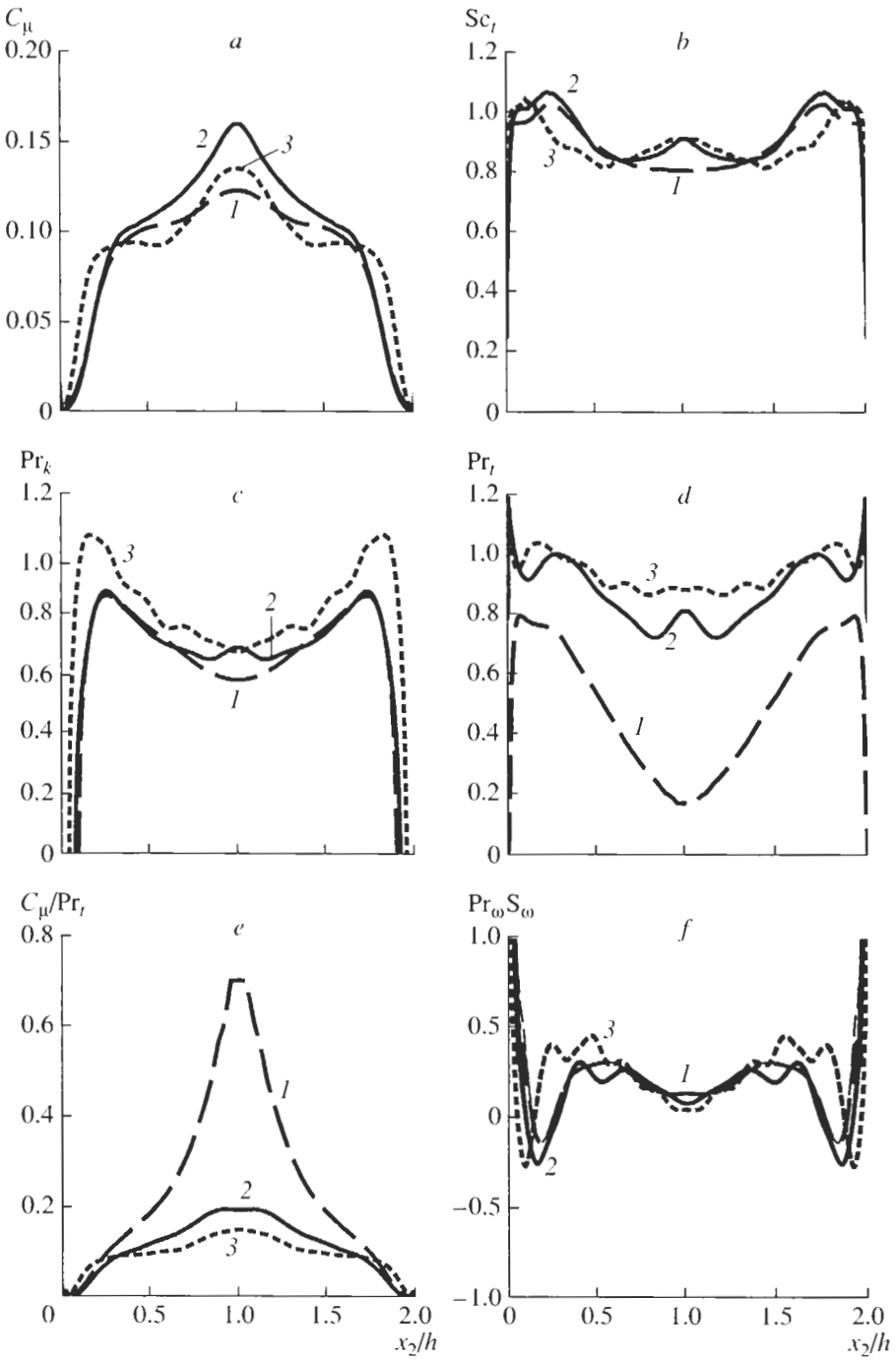

Fig. 3. DNS data as given in Fig. 2 but now for the turbulence model parameters C_μ (*a*) Sc_t (*b*), Pr_k (*c*), Pr_t (*d*) and C_μ/Pr_t (*e*). $Pr_\omega S_\omega$ is shown in fig. *f*, where two values for Pr_ω are applied: $Pr_\omega = 0.6$ and $Pr_\omega = 0.9$.

2.4. The turbulence model parameters

The result of computing the turbulence model parameters by means of the DNS data is shown in Fig. 3. C_μ, which is usually approximated by the constant value $C_\mu = 0.09$ [1, 13], shows significant variations with the normalized wall distance x_2/h. The Mach number increase implies a somewhat higher standardized turbulent transport efficiency C_μ, which appears to be plausible. The Reynolds number increase has a significant effect: the CH plateau is much more pronounced than for the IL and CL cases. This behavior is similar to the features found for the production-to-dissipation ratio P/ε of turbulent kinetic energy and $S\tau$, see Fig. 2.

The results found for the Prandtl numbers Sc_t, Pr_k and Pr_t in the mass fraction, turbulent kinetic energy and temperature equation, respectively, reveal the fol-

lowing. The effect of compressibility is small with regard to Sc_t and Pr_k, but there is a relevant influence on Pr_t which is much higher for compressible than for incompressible flows. This means that the stronger coupling of the transport of momentum and heat in compressible flows hampers the standardized turbulent energy transport efficiency C_μ/Pr_t, which is a plausible result. The Reynolds number has a similar effect on Pr_k and Pr_t: their values are closer to unity, this means the difference between the turbulent transport of turbulent kinetic energy and temperature to the turbulent momentum transport becomes smaller. The effect of the Reynolds number on Sc_t is smaller than its effect on Pr_k and Pr_t, which may be related to the fact that the IL and CL values for Sc_t are already close to unity.

$Pr_\omega S_\omega$ is shown in dependence on Pr_ω, which is considered to be constant. The values $Pr_\omega = 0.6$ and $Pr_\omega = 0.9$ applied correspond to an appropriate range of variations of this quantity. A relevant (and somewhat surprising) finding is that the compressibility effect on $Pr_\omega S_\omega$ is rather small, *i.e.*, compressibility does not affect the generation mechanism of turbulence frequency. In contrast to that, the Reynolds number increase has a significant structural effect: the source rate distribution becomes smoother. This feature agrees again well with similar findings for the production-to-dissipation ratio P/ε, time scale ratio $S\tau$ and C_μ.

The findings obtained for the turbulence model parameters can be used as guideline for the development of a turbulence model, which requires parameterizations of model parameters in terms of quantities that are available in simulations. This analysis reveals that the use of the effective value $Pr_t = Pr_k = Sc_t = 0.9$ for the Prandtl numbers in the temperature, turbulent kinetic energy and scalar equations, respectively, is well justified. No support is found for the usual practice of modeling C_μ and S_ω: C_μ does not scale with the turbulence Reynolds number Re_L, and the model (2.10) disagrees with the DNS results. Instead, one finds that the parameterizations $C_\mu = 0.16\exp(-(i/0.09)^2)$ and $Pr_\omega S_\omega = \tau_*^{-0.22}(0.34 - 0.54\tau_*)$ work very well. Here, $i = (2k/3)^{1/2}/\overline{U}_1$ refers to the turbulence intensity, and $\tau_* = 0.37[1 - (x_2/h - 1)^2]$ denotes a characteristic dimensionless time scale. Combined with $Pr_\omega = 0.9$, the performance of the resulting turbulence model is very good: there are hardly differences to the DNS results. All the details of this analysis may be found elsewhere [14].

3. SCALAR PDF EQUATIONS

Next, we consider the second question pointed out in the introduction: the modeling of scalar mixing. The model that is used in general for that is the "interaction by exchange with the mean" (IEM) model [15]. The problem related to this model is that the influence of noise on the scalar evolution is not considered. Non-premixed combustion problems are often characterized by the appearance of strongly non-Gaussian (bimodal) initial PDFs, which evolve towards equilibrium (Gaussian) PDFs. This transition cannot be described in terms of the IEM model. The lack of noise generation implies that information about the initial state is never lost: the standardized scalar PDF does not change in time [15]. In general, the consideration of a noise term that is independent of the actual scalar value is not an appropriate way to overcome this problem [16, 17]. Scalars have the characteristic property to be bounded: the convex region in sample space occupied by the scalars decreases with time [1]. This property cannot be satisfied if such a noise term is applied because unphysical scalar values outside of bounds may appear.

To describe both the loss of information about the initial state and the boundedness of scalars one needs a stochastic forcing in scalar equations that depends on the scalar – the noise term has to vanish for scalar values near bounds. The consideration of such noise processes has significant consequences. In general, scalars are found to be correlated over finite times (for example due to transport within one eddy). Thus, stochastic forces that involve scalars have to be correlated over finite times, too. A methodology to obtain such generalized stochastic equations is the projection operator technique. It enables the extraction of the dynamics of relevant variables from underlying deterministic dynamics of (microscopic) quantities [18–21]. In agreement with the requirements described above, the dynamics of variables considered are found to be driven by correlated stochastic forces.

3.1. Generalized stochastic equations

The application of the projection operator technique to the problem considered will be described now. To keep the development simple, we restrict the attention to the transport of a passive, inert scalar in statistically homogeneous velocity and scalar fields. In this case, the projection operator technique provides equations for the transport of a scalar Φ^*, which may be written [22]

$$\frac{d\Phi^*}{dt} = \Psi^*, \tag{3.1a}$$

$$\frac{d\Psi^*}{dt} = -A\Psi^* - B\Phi^* + C\frac{dW}{dt}. \tag{3.1b}$$

The scalar derivative Ψ^* is defined by (3.1a). A, B and C are any deterministic functions of Φ^*, Ψ^* and t; dW/dt is a Gaussian process with vanishing mean, $\langle dW/dt\rangle = 0$, and uncorrelated values at different times, $\langle dW/dt(t)dW/dt'(t')\rangle = \delta(t - t')$, where $\delta(t - t')$ is the delta function. The averages $\overline{\Phi}$ and $\overline{\Psi}$ have to be constant for the flow considered. For simplicity, they are set equal to zero.

To explain the physics of (3.1a, b), it is advantageous to rewrite these equations into a standardized form. We define a characteristic scalar variance decay time scale τ_φ in terms of the scalar variance,

$$\frac{1}{\tau_\varphi} = -\frac{1}{2\overline{\phi^2}}\frac{d\overline{\phi^2}}{dt}, \qquad (3.2)$$

where ϕ denotes the scalar fluctuation. The introduction of τ_φ enables the definition of a dimensionless time scale

$$T = 2\int_0^t ds\,\tau_\varphi^{-1}.$$

Equation (3.2) then provides $\overline{\phi^2} = \overline{\phi^2(0)}\exp(-T)$. By adopting this expression, we can rewrite the Eqs. (3.1a, b) in terms of the standardized variables $\hat{\phi} = \Phi^*/\overline{\phi^2}^{1/2}$ and $\hat{\psi} = 0.5\hat{\phi} + 0.5\tau_\varphi\Psi^*/\overline{\phi^2}^{1/2}$,

$$\frac{d\hat{\phi}}{dT} = \hat{\psi}, \qquad (3.3a)$$

$$\frac{d\hat{\psi}}{dT} = a\left\{-\hat{\psi} - b\hat{\phi} + c\frac{dW}{dT}\right\}. \qquad (3.3b)$$

In (3.3b), we introduced the coefficients $a = (\tau_\varphi A - d\tau_\varphi/dt)/2 - 1$, $b = (\tau_\varphi^2 B - 2A + 1)/(4a)$ and $c = C\tau_\varphi^{1/2}/(2a^2\overline{\phi^2})^{1/2}$.

We consider the transport equations for the variances of $\hat{\phi}$ and $\hat{\psi}$ in order to derive constraints for the coefficients a and b. These variance equations can be obtained by adopting the PDF transport equation that corresponds to the stochastic Eqs. (3.3a, b). The applied normalization implies that $\overline{\hat{\phi}^2} = 1$. The transport equation for $\overline{\hat{\phi}^2}$ then leads to $\overline{\hat{\phi}\hat{\psi}} = 0$, and the transport equation for $\overline{\hat{\phi}\hat{\psi}}$ implies the consistency constraint

$$b = a^{-1}\overline{\hat{\psi}^2}, \qquad (3.4)$$

which determines the coefficient b. The transport equation for $\overline{\hat{\psi}^2}$ reads

$$\frac{d\overline{\hat{\psi}^2}}{dT} = -2a\overline{\hat{\psi}^2} + a^2c^2. \qquad (3.5)$$

The coefficient a is considered as a constant fitting parameter.

3.2. The scalar dynamics

The consideration of the model (3.1a, b) in its standardized form (3.3a, b) simplifies the explanation of the physics described in this way. For doing this, we will rewrite (3.3a, b) into one equation for the scalar $\hat{\phi}$. First, we solve (3.3b) formally, which results in

$$\hat{\psi} = -\int_0^T dT'\exp\{-a(T-T')\}\overline{\hat{\psi}^2}(T')\hat{\phi}(T') + f(T), \qquad (3.6a)$$

$$f(T) = a\int_0^T dT'\exp\{-a(T-T')\}c(T')\frac{dW}{dT'}(T'). \qquad (3.6b)$$

To obtain (3.6a), we applied $\hat{\psi}(0) = 0$ which assures that $\overline{\hat{\phi}\hat{\psi}} = 0$. Further, we used $b = \overline{\hat{\psi}^2}/a$ to replace b, and we introduced the abbreviation $f(T)$ that is given through (3.6b). The function $f(T)$ vanishes in the mean, and its correlation function is given according to (3.6b) by

$$\overline{f(T)f(T')} = \overline{\hat{\psi}^2}(T')\exp\{-a(T-T')\}, \qquad (3.7)$$

where $T \geq T'$ is assumed. The consistency of (3.7) at $T = T'$ can be seen by proving that $\overline{f^2(T')}$ satisfies the same transport equation as $\overline{\hat{\psi}^2}(T')$. Therefore, these two functions must be equal because $\overline{\hat{\psi}^2}$ vanishes initially as $\overline{f^2(T')}$. The use of (3.6a) combined with (3.7) in (3.3a) then results in the following form of the model (3.3a, b),

$$\frac{d\hat{\phi}}{dT} = -\int_0^T dT'\,\overline{f(T)f(T')}\hat{\phi}(T') + f(T), \qquad (3.8a)$$

$$\frac{df}{dT} = -af + ac\frac{dW}{dT}, \qquad (3.8b)$$

where (3.6b) is used to obtain (3.8b). To be consistent with (3.6b), we have to demand that $f(0) = 0$.

We observe that the scalar Eq. (3.8a) is fully determined through the properties of the stochastic force f. This force simulates stochastic motions that appear randomly and disappear with a characteristic time scale a^{-1}. The generation and decay of these stochastic motions are modeled through the right-hand side of Eq. (3.8b). In agreement with the requirements pointed out above, the scalar dynamics are found to be driven by correlated stochastic forces. The consideration of such memory effects regarding the forcing has to be complemented by their incorporation into the relaxation term (the first term on the right-hand side of (3.8a)).

It is worth noting that the model (3.8a, b) reduces asymptotically to an extension of the IEM model. In the

limit of a vanishing correlation time $a^{-1} \longrightarrow 0$, the force f becomes delta-correlated,

$$\overline{f(T)f(T')} = \frac{2}{a}\overline{\hat{\psi}^2}(T')\delta(T-T') = \\ = \overline{c^2}(T)\delta(T-T'). \tag{3.9}$$

The last expression is found by adopting the relation (3.5) in the limit $a^{-1} \longrightarrow 0$, which is equivalent to neglecting the derivative on the left-hand side. The use of (3.9) in (3.8a) then results in

$$\frac{d\hat{\phi}}{dT} = -\frac{\overline{c^2}}{2}\hat{\phi} + c\frac{dW}{dT}. \tag{3.10}$$

This model generalizes the IEM model, which follows by setting $c = 0$. In this case, information about structures of the initial scalar PDF will not disappear in time, which is the well-known drawback of the IEM model [1, 15].

3.3. The modeling of c

An important property of scalars is their characteristic boundedness [1, 15], which has implications for the modeling of c in (3.3b): the application of a coefficient c that is independent of the actual scalar value results in the appearance of unphysical scalar values outside of bounds. The boundedness constraint could be satisfied within the frame of Fokker-Planck equations by adopting boundary conditions [16, 23–25]. The suitability of simulating the flows considered by Juneja and Pope [26] in conjunction with reflection conditions at boundaries [16, 23] was investigated in preparation of the calculations described below. It was found that the significant overprediction of the PDF structure decay in the outer parts of the scalar PDF, which is observed if boundary conditions are not applied, can be limited in this way but this leads to the appearance of unphysical peaks of the PDFs at the boundaries.

Another way to guarantee the boundedness of scalar values consists in an appropriate specification of the coefficient c. This will be done here by assuming that c is nonzero only inside the lower and upper bounds of the scalar space $\hat{\phi}_-$ and $\hat{\phi}_+$, respectively, and given by the relation

$$c^2 = C^*_{\varphi 0}[(\hat{\phi}-\hat{\phi}_-)(\hat{\phi}_+-\hat{\phi})]^n; \tag{3.11}$$

$C^*_{\varphi 0}$ is a proportionality factor that will be calculated below. The power n can be determined by the following arguments. One may easily check that the maximum of c^2 is given by

$$c^2_{max} = C^*_{\varphi 0}\left(\frac{\hat{\phi}_+ - \hat{\phi}_-}{2}\right)^{2n}. \tag{3.12}$$

The asymptotic model (3.10) reveals that $\overline{c^2}$ represents a characteristic frequency of the scalar relaxation. One has to expect this frequency $\overline{c^2}$ as the sum of independent contributions related to the lower and upper bounds. This implies $n = 0.5$ so that

$$c^2 = C^*_{\varphi 0}[(\hat{\phi}-\hat{\phi}_-)(\hat{\phi}_+-\hat{\phi})]^{1/2}. \tag{3.13}$$

The remaining question is the modeling of the evolution of the bounds $\hat{\phi}_-$ and $\hat{\phi}_+$. These functions have to satisfy deterministic equations, which should be linear in $\hat{\phi}_-$ and $\hat{\phi}_+$ according to the linear deterministic contributions in (3.3a, b). Hence, we postulate

$$\frac{d}{dT}\hat{\phi}_\pm = \lambda\hat{\phi}_\pm, \tag{3.14}$$

where λ is a constant that has to be determined. The integration of (3.14) provides

$$\hat{\phi}_\pm(T) = \hat{\phi}_\pm(0)\exp(\lambda T). \tag{3.15}$$

The model (3.3a, b) in conjunction with $b = \overline{\hat{\psi}^2}/a$, (3.13) and (3.15) will be referred to below as "refined interaction by exchange with the mean" (RIEM) model. It guarantees the boundedness of scalars statistically: some scalar values may be found outside the bounds but the probability for such events is very small. This will be demonstrated by comparisons with DNS data below.

3.4. Comparison with DNS

The RIEM model will be tested by the comparison with the R92A-DNS data of scalar mixing in stationary, homogeneous and isotropic turbulence obtained by Juneja and Pope [26]. The Taylor-scale Reynolds number is $\mathrm{Re}_\lambda = 92$ in this simulation. Two initial PDFs $f_\varphi(\theta, t) = \overline{\delta(\phi(t)-\theta)}$ were considered close to $f_\varphi = [\delta(\theta - \sqrt{3}/2) + \delta(\theta + \sqrt{3}/2) + \delta(\theta)]/3$ (scalar 1) and $f_\varphi = [\delta(\theta - 1) + 2\delta(\theta + 0.5)]/3$ (scalar 2). It is worth emphasizing that the prediction of the evolution of these scalar fields is remarkably more challenging than previous comparisons with the DNS data of Eswaran and Pope [27]: the symmetric scalar–1 PDF contains modes which decay differently, and the scalar-2 PDF is strongly asymmetric.

The PDF evolution was considered in terms of the normalized scalar variance Φ_T defined by $\Phi_T^2 = \overline{\phi^2(T)}/\overline{\phi^2(0)} = e^{-T}$. This quantity is bounded, $0 \le \Phi_T \le 1$. The initial values for $\hat{\phi}$ were chosen according to the DNS data for $\Phi_T = 1$. The $\hat{\psi}$-values were set equal to zero initially to satisfy the condition $\overline{\hat{\phi}\hat{\psi}} = 0$. The equations (3.3a, b) were solved numerically by

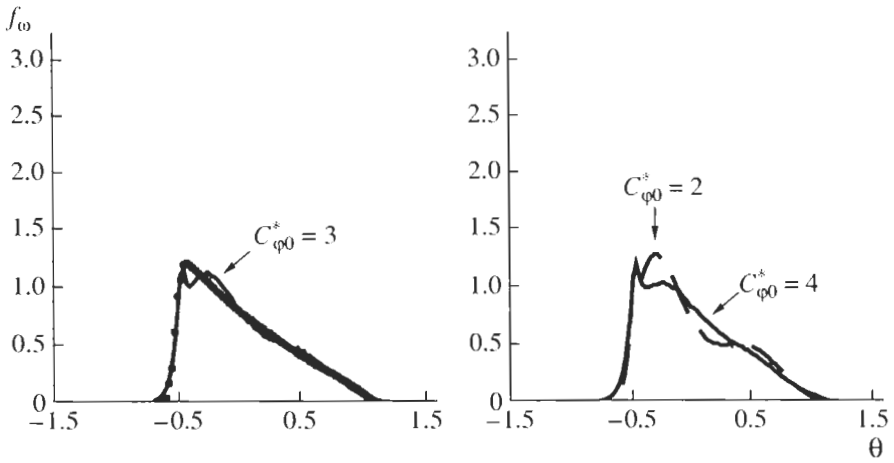

Fig. 4. The RIEM model prediction (line) with $C^*_{\varphi 0} = 3$ is compared to Juneja and Pope's [26] DNS data of the scalar-2 PDF (dots) at $\Phi_T = 0.6$ in fig. *a*. The effect of $C^*_{\varphi 0}$-variations is shown in fig. *b*.

adopting $5 \cdot 10^5$ particles and a time step $dT = 0.002$. At the corresponding Φ_T, $f_\varphi(\theta)$ was calculated where intervals $\Delta\theta = 0.025$ were applied to calculate the value of f_φ at θ. The parameters of the bound model (3.15) were found by means of the DNS-data as $\lambda = 0.3$, $\hat{\phi}_-(0) = -1.90$ and $\hat{\phi}_+(0) = 1.90$ (scalar 1), $\hat{\phi}_-(0) = -0.93$ and $\hat{\phi}_+(0) = 2.08$ (scalar 2). The parameters a and $C^*_{\varphi 0}$ were fitted to achieve the best agreement with the DNS data. The value $a = 1$ was found as an optimal value. Figure 4*a* demonstrates the good performance of PDF simulations where $C^*_{\varphi 0} = 3$ was used. The effect of $C^*_{\varphi 0}$–variations is shown in Fig. 4*b*. Only the scalar-2 DNS data were used to determine the model parameters. Hence, the assessment of PDF calculations of the scalar-1 evolution can be performed with independent data.

The Figs. 5 and 6 show that the results of these PDF simulations agree well with the corresponding DNS data. The most difficult task is the simulation of the non-equilibrium processes within the first stage of mixing, $0.7 \le \Phi_T \le 1$. The results of the PDF simulations are very similar as the DNS data, there are only minor differences. The mixing processes may be seen to be in the near-equilibrium stage for $\Phi_T \le 0.6$, where T becomes greater than $a^{-1} = 1$. Here, the RIEM model predicts approximately the same PDF as found by DNS. The relevance of memory effects can be assessed through a comparison with the performance of the asymptotic model (3.10) combined with a constant c. For the latter, one finds an optimal value $c = 0.65$, which provides the best agreement between the model prediction and the scalar-2 DNS data at $\Phi_T = 0.6$. The resulting scalar PDF calculations are also shown in the Figs. 5 and 6. These figures reveal significant deviations between the predictions of the RIEM and asymptotic model (3.10) in the early stage of mixing ($0.7 \le \Phi_T \le 1$). For $\Phi_T \le 0.6$, one finds that the predictions of both models are very similar, in particular for the scalar-1 case. This shows that memory effects are of minor relevance in this stage of mixing.

The comparison of the joint scalar PDF predicted by the RIEM model with the corresponding DNS data of Juneja and Pope [26] reveals that the RIEM model satisfies the boundedness constraint, *i.e.*, the convex region in sample space occupied by the scalars decreases with time. The details of these comparisons may be found elsewhere [28].

4. FDF EQUATIONS

The RANS and PDF methods described above reveal that one has to apply flow-dependent models in general, which may have a relatively complex structure. Such models have a limited predictive power – one has to provide evidence for such predictions which often represents a non-trivial problem. As an alternative to RANS methods, one may apply Large Eddy Simulation (LES). Large-scale processes are resolved without approximations within this approach, which enables predictions that are often found to be more accurate than those of RANS equations [1, 29–31]. Nevertheless, the use of LES requires the modeling of Subgrid Scale (SGS) processes. For this reason, the application of LES to reacting flows is faced with the same problem as the use of RANS methods: such LES equations are characterized by the appearance of unknown filtered reaction rates for which accurate parameterizations are unavailable in general. A way to overcome this problem is the use of the PDF methodology to extend LES equations to equations for instantaneous velocities and scalars. This was suggested by Givi [32] and applied first by Madnia and Givi [33]. Pope [34] introduced the concept of a FDF which is essentially the PDF of SGS variables. He showed that the use of this methodology offers for reacting flow simulations the

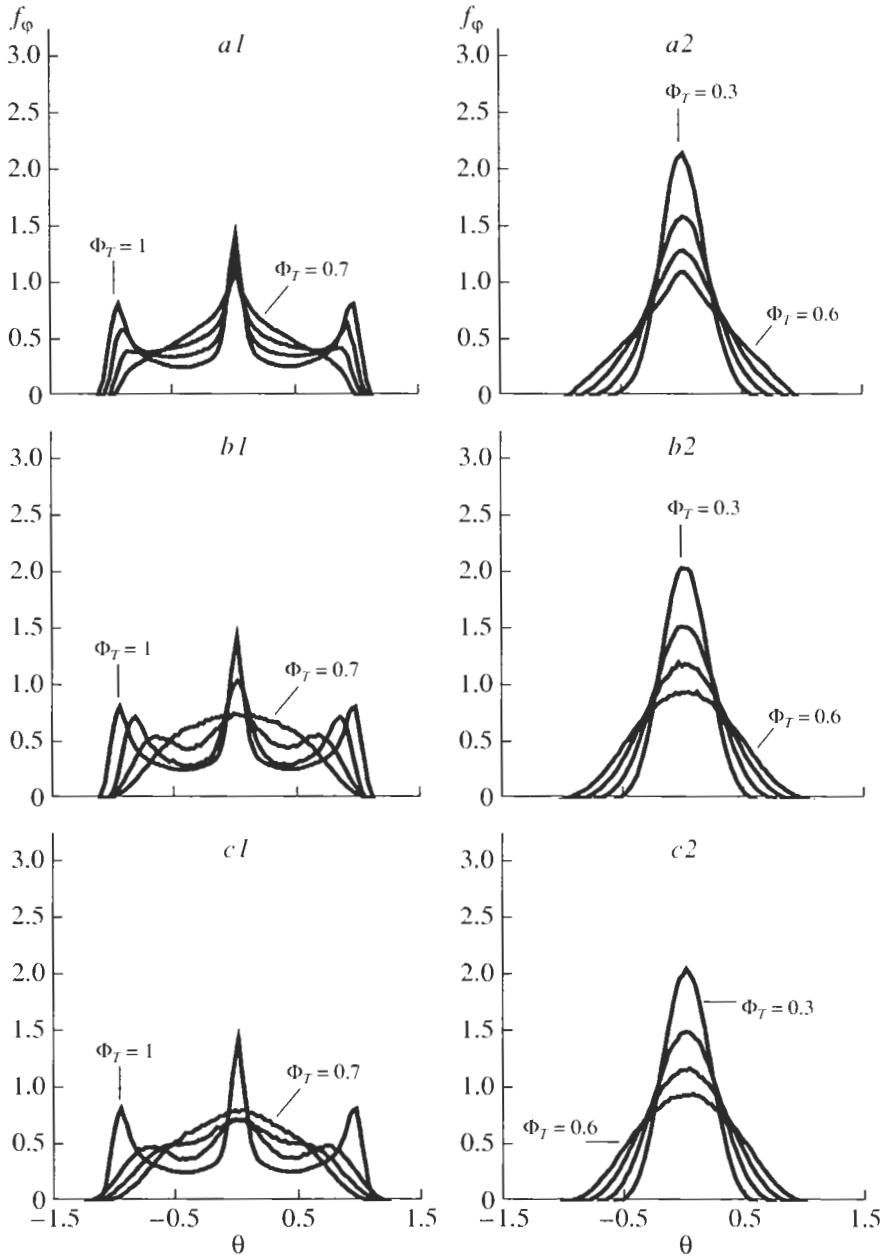

Fig. 5. The scalar-1 PDF evolution in stationary, homogeneous and isotropic turbulence is given in figs. *a1* and *a2* according to the DNS data of Juneja and Pope [26]. The corresponding predictions of the RIEM model are shown in figs. *b1* and *b2*, where $C^*_{\varphi 0} = 3$ is applied. The figs. *c1* and *c2* show the predictions of the asymptotic model (3.10) combined with $c = 0.65$.

same advantage as the use of PDF methods: chemical reactions appear in a closed form. Gao and O'Brien [35] developed a transport equation for the scalar FDF and offered suggestions for modeling of the unclosed terms in this equation.

One way to use FDF methods is their application to flow simulations. Basically, this was done recently by adopting hybrid FDF methods where the velocity field is calculated by means of conventional LES equations and the scalar transport by a FDF transport equation [36–39]. Such methods apply algebraic approximations to close the SGS scalar flux in terms of scalar gradients. A more general approach consists in the stochastic simulation of both velocity and scalar fields. Such calculations are feasible as shown by Gicquel *et al.* [40] who performed the first FDF simulations of velocity fields (scalars were not involved). Nevertheless, it turned out that the effort related to the use of velocity-scalar FDF methods is very high. The simulation of velocity fields is 6 times less expensive than DNS, but it requires 15–30 times more effort than LES methods [40].

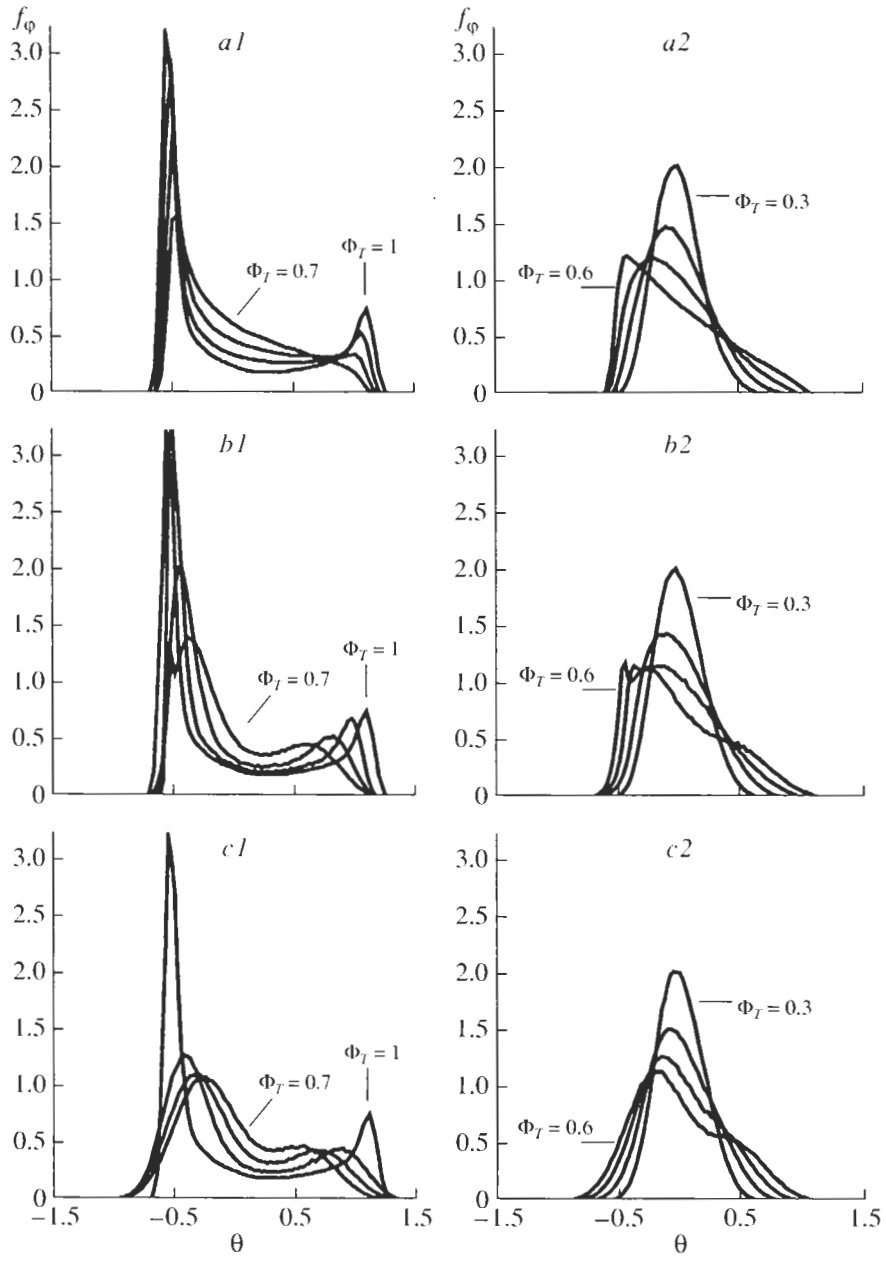

Fig. 6. The same comparison as in Fig. 5, but with reference to the scalar-2 PDF.

Another way to use FDF methods for velocities and scalars is their application to the construction of simpler (hybrid) FDF methods, which are more efficient. This question will be addressed here. First, this is done to improve existing velocity LES and scalar FDF methods by assuring the consistency of these methods. This means, for instance, that the same model for instantaneous velocities is used to calculate (within the frame of a hybrid method) filtered velocities and the transport of scalars in physical space, or different contributions to algebraic expressions for the SGS stress tensor. The application of such consistent methods was found to be of remarkable relevance to the use of PDF methods [41–43], so that the same may be expected with regard to the use of FDF methods. The second reason for performing this analysis is the possibility to assess FDF models for velocities and scalars through the comparison of their implications with well-investigated phenomenological models. This complements their assessment by means of specific flow simulations. It enables more general insight into the suitability of models and the choice of model parameters (e.g., for the case that backscatter effects have to be involved).

The LES equations will be presented in section 4.1. Their closure requires their extension to a stochastic model. This will be presented in section 4.2. Section

4.3 shows how this stochastic model can be reduced to consistent LES equations for the velocity field. The closure of scalar equations is then the concern of sections 4.4 and 4.5.

4.1. The LES equations

The mass density-weighted filtered value of any function Q of velocities $\mathbf{U}(\mathbf{x}, t) = (U_1, U_2, U_3)$ and scalars (the mass fractions of N species and temperature) $\mathbf{\Phi}(\mathbf{x}, t) = (\Phi_1, \ldots, \Phi_{N+1})$ will be defined by

$$\overline{Q} = \langle\rho\rangle^{-1}\langle\rho Q\rangle. \tag{4.1}$$

Here, $\rho(\mathbf{x}, t)$ is written for the mass density, and the bracket refers to a spatial filtering,

$$\langle\rho(\mathbf{x}, t)Q(\mathbf{x}, t)\rangle = \int d\mathbf{r}\rho(\mathbf{x}-\mathbf{r}, t)Q(\mathbf{x}-\mathbf{r}, t)G(\mathbf{r}). \tag{4.2}$$

The filter function G is assumed to be homogeneous. We assume that $\int d\mathbf{r}\, G(\mathbf{r}) = 1$ and $G(\mathbf{r}) = G(-\mathbf{r})$. Only positive filter functions [44] are considered for which all the moments $\int d\mathbf{r}\, r^m G(\mathbf{r})$ exist for $m \geq 0$ [36].

The filtering of the basic equations results in the following LES equations for the filtered mass density $\langle\rho\rangle$, velocities $\overline{U}_i$ and scalars $\overline{\Phi}_\alpha$,

$$\frac{\partial\langle\rho\rangle}{\partial t} + \frac{\partial\langle\rho\rangle\overline{U}_k}{\partial x_k} = 0, \tag{4.3a}$$

$$\frac{\partial\overline{U}_i}{\partial t} + \overline{U}_k\frac{\partial\overline{U}_i}{\partial x_k} + \langle\rho\rangle^{-1}\frac{\partial\langle\rho\rangle\overline{u_k u_i}}{\partial x_k} = \\ = 2\langle\rho\rangle^{-1}\frac{\partial}{\partial x_k}\langle\rho\rangle\nu\left(\bar{S}_{ik} - \frac{1}{3}\bar{S}_{nn}\delta_{ik}\right) - \langle\rho\rangle^{-1}\frac{\partial\langle p\rangle}{\partial x_i} + \bar{F}_i, \tag{4.3b}$$

$$\frac{\partial\overline{\Phi}_\alpha}{\partial t} + \overline{U}_k\frac{\partial\overline{\Phi}_\alpha}{\partial x_k} + \langle\rho\rangle^{-1}\frac{\partial\langle\rho\rangle\overline{u_k\phi_\alpha}}{\partial x_k} = \\ = \langle\rho\rangle^{-1}\frac{\partial}{\partial x_k}\langle\rho\rangle\nu_{(\alpha)}\frac{\partial\overline{\Phi}_\alpha}{\partial x_k} + \bar{S}_\alpha. \tag{4.3c}$$

Repeated indices imply summation with the exception of subscripts in parentheses. F_i is any external force (the acceleration due to gravity), $p = p(\rho, \mathbf{\Phi})$ the pressure that is defined via the thermal equation of state, and S_α denotes a known source rate. $S_{ik} = (1/2)[\partial U_i/\partial x_k + \partial U_k/\partial x_i]$ is the rate-of-strain tensor and ν the kinematic viscosity, which is considered to be constant for simplicity. $\nu_{(\alpha)}$ is the molecular or thermal diffusivity of the scalar Φ_α. To derive the first term on the right-hand side of the equation (4.3b), we assumed that $\overline{\partial U_i/\partial x_k} = \partial\overline{U}_i/\partial x_k$. A corresponding relation is assumed regarding the derivation of the first term on the right-hand side of (4.3c). The expressions $\overline{u_k u_i}$ and $\overline{u_k\phi_\alpha}$ on the left-hand sides of (4.3b, c) are called the SGS stress tensor and SGS scalar flux. Within the frame of RANS and PDF methods, one often considers u_i and ϕ_α to be the fluctuations of U_i and Φ_α. This is not done here but $\overline{u_k u_i}$ and $\overline{u_k\phi_\alpha}$ (and corresponding expressions that involve u_i and ϕ_α) are seen as symbols, which are defined by the following expanded forms,

$$\overline{u_k u_i} = \overline{U_k U_i} - \overline{U}_k\overline{U}_i, \quad \overline{u_k\Phi_\alpha} = \overline{U_k\Phi_\alpha} - \overline{U}_k\overline{\Phi}_\alpha. \tag{4.4}$$

The purpose of defining $\overline{u_k u_i}$ and $\overline{u_k\phi_\alpha}$ in this way is to avoid the appearance of double-filtering operations $\overline{\overline{U}}_k$ and $\overline{\overline{\Phi}}_\alpha$ because $\overline{U}_k \neq \overline{\overline{U}}_k$ and $\overline{\Phi}_\alpha \neq \overline{\overline{\Phi}}_\alpha$ in general [1].

The problem that has to be solved to apply the Eqs. (4.3a–c) to turbulent reacting flow simulations is to provide closures for the unknowns $\overline{u_k u_i}$, $\overline{u_k\phi_\alpha}$ and $\bar{S}_\alpha$. To calculate these terms, one has to assess the effects of fluctuations on $\overline{U_k U_i}$, $\overline{U_k\Phi_\alpha}$ and $\bar{S}_\alpha$, which requires a model for both the dynamics of resolved variables $\overline{U}_i$, $\overline{\Phi}_\alpha$ and fluctuations around these variables. Such a model for the dynamics of instantaneous velocities and scalars will be presented next.

4.2. The stochastic model

The model for instantaneous velocities U_i^* $(i = 1, 3)$ and scalars Φ_α^* $(\alpha = 1, N+1)$ is considered within the Lagrangian framework, where particle positions x_i^* are involved as independent variables,

$$\frac{d}{dt}x_i^* = U_i^*, \tag{4.5a}$$

$$\frac{d}{dt}U_i^* = \bar{\Gamma}_i + \bar{F}_i - \frac{1}{\tau_L}(U_i^* - \overline{U}_i) + \sqrt{C_0\varepsilon_r}\frac{dW_i}{dt}, \tag{4.5b}$$

$$\frac{d}{dt}\Phi_\alpha^* = \bar{\Omega}_\alpha + S_\alpha - \frac{1}{\tau_\varphi}(\Phi_\alpha^* - \overline{\Phi}_\alpha) + \\ + G_{\alpha m}(U_m^* - \overline{U}_m). \tag{4.5c}$$

$\bar{\Gamma}_i$ plus $\bar{F}_i$ and $\bar{\Omega}_\alpha$ plus $\bar{S}_\alpha$ determine the dynamics of resolved velocities $\overline{U}_i$ and scalars $\overline{\Phi}_\alpha$, as may be seen by filtering these equations. According to (4.3b, c) one finds [28]

$$\bar{\Gamma}_i = 2\langle\rho\rangle^{-1}\frac{\partial}{\partial x_k}\langle\rho\rangle\nu\left(\bar{S}_{ik} - \frac{1}{3}\bar{S}_{nn}\delta_{ik}\right) - \langle\rho\rangle^{-1}\frac{\partial\langle p\rangle}{\partial x_i}, \\ \bar{\Omega}_\alpha = \langle\rho\rangle^{-1}\frac{\partial}{\partial x_k}\langle\rho\rangle\nu_{(\alpha)}\frac{\partial\overline{\Phi}_\alpha}{\partial x_k}. \tag{4.6}$$

The body force in the velocity equation (4.5b) is assumed to be independent of velocities and scalars, $F_i = \overline{F}_i$. This simplifies the explanations given below because $\overline{F}_i$ does not affect the calculation of the SGS stress tensor. The Boussinesq approximation [28] is not covered in this way. There is no need for doing this because compressibility effects can be taken into account as shown below. No assumption is made regarding the source term S_α in the scalar equation (4.5c).

The remaining terms on the right-hand sides of (4.5b, c) model the dynamics of velocity and scalar fluctuations. Velocity fluctuations are assumed to be generated by the last term in (4.5b). dW_i/dt is a Gaussian process with vanishing means, $\langle dW_i/dt\rangle = 0$, and uncorrelated values at different times, $\langle (dW_i/dt(t))dW_j/dt'(t')\rangle = \delta_{ij}\delta(t-t')$. The symbol δ_{ij} is the Kronecker delta and $\delta(t-t')$ the delta function. The coefficient of dWi/dt has the same structure as applied in PDF methods [1]. The SGS dissipation rate of turbulent kinetic energy ε_r will be defined below, and C_0 is a constant that has to be estimated. A corresponding stochastic source term in the scalar equation (4.5c) is not considered. Such a term is needed within the frame of PDF methods to simulate the loss of information about the initial PDF in time [28]. However, there is no need to consider such a term in FDF methods because most of the scalar spectrum is resolved. The effect of noise on the scalar dynamics is involved in (4.5c) via the term related to velocity fluctuations. The appearance of this term is a consequence of assuming a locally isotropic dissipation of the scalar field. Accordingly, $G_{\alpha m}$ is determined by [28]

$$G_{\alpha m} = \frac{1}{\tau_\varphi}\overline{\phi_\alpha u_i}V^{-1}_{im}; \tag{4.7}$$

V^{-1} refers to the inverse velocity variance matrix V which has elements $V_{ij} = \overline{u_i u_j}$. The third terms on the right-hand sides of (4.5b, c) involve the most relevant assumptions. They model the relaxation of velocity and scalar fluctuations. It is assumed here that velocity and scalar fluctuations relax only in interaction with their own means, where τ_L and τ_φ are characteristic relaxation times that have to be estimated.

The Eqs. (4.5a–c) for the dynamics of SGS fluctuations were validated through simulations of various two-dimensional jets and mixing layers and a three-dimensional temporally developing mixing layer. The good performance of the velocity Eq. (4.5b) (without body force) was proved by Gicquel *et al.* [40]. The performance of the scalar Eq. (4.5c) combined with a conventional LES equation for the velocity field was investigated by Colucci *et al.* [36], Jaberi *et al.* [37] and Zhou and Pereira [39]. The term that involves velocity fluctuations in (4.5c) had to be neglected in these simulations because velocity fluctuations were not incorporated into the stochastic model. The consideration of the Eqs. (4.5a–c) can also be justified with the argument that their analysis is equivalent to the consideration of a limiting case: the Eqs. (4.5a–c) represent the simplest possible model for the dynamics of SGS fluctuations that can be applied.

It is worth emphasizing that the solution of (4.5a–c) overcomes the closure problems related to the LES Eqs. (4.3a–c). The Eqs. (4.5a–c) are closed for specified τ_L, τ_φ and C_0, and the expressions (4.6) assure that the transport of filtered quantities is calculated according to (4.3a–c). However, the solution of (4.5a–c) is very expensive. Thus, for reasons given in the introduction these equations will be reduced to simpler methods.

4.3. The closure of LES equations

The stochastic model (4.5a–c) determines the joint velocity-scalar FDF that is defined by

$$F(\mathbf{v}, \boldsymbol{\theta}, \mathbf{x}, t) = \overline{\delta(\mathbf{U}(\mathbf{x}, t) - \mathbf{v})\delta(\boldsymbol{\Phi}(\mathbf{x}, t) - \theta)}. \tag{4.8}$$

Its transport equation can be derived from (4.5a–c) by means of standard methods. It reads [1, 24, 25]

$$\begin{aligned}\frac{\partial}{\partial t}\langle\rho\rangle F + \frac{\partial}{\partial x_i}\langle\rho\rangle v_i F = \\ = -\frac{\partial}{\partial v_i}\langle\rho\rangle\left[\overline{\Gamma}_i - \frac{1}{\tau_L}(v_i - \overline{U}_i) + \overline{F}_i\right]F + \\ + \frac{\partial^2}{\partial v_j \partial v_j}\langle\rho\rangle\frac{C_0\varepsilon_r}{2}F - \\ - \frac{\partial}{\partial\theta_\alpha}\langle\rho\rangle\left[\overline{\Omega}_\alpha - \frac{1}{\tau_\varphi}(\theta_\alpha - \overline{\Phi}_\alpha) + G_{\alpha m}(v_m - \overline{U}_m) + S_\alpha\right]F.\end{aligned} \tag{4.9}$$

By multiplying (4.9) with $v_i v_j$ and integrating it over the velocity-scalar space, one may derive the following equation for the SGS stress tensor $\overline{u_i u_j}$,

$$\begin{aligned}\frac{\partial\overline{u_i u_j}}{\partial t} + \overline{U}_k\frac{\partial\overline{u_i u_j}}{\partial x_k} + \langle\rho\rangle^{-1}\frac{\partial\langle\rho\rangle\overline{u_k u_i u_j}}{\partial x_k} + \overline{u_k u_j}\frac{\partial\overline{U}_i}{\partial x_k} + \\ + \overline{u_k u_i}\frac{\partial\overline{U}_j}{\partial x_k} = -\frac{2}{\tau_L}\overline{u_i u_j} + C_0\varepsilon_r\delta_{ij}.\end{aligned} \tag{4.10}$$

In an analogous manner as the SGS stress tensor, the term $\overline{u_k u_i u_j}$ is defined by

$$\begin{aligned}\overline{u_k u_i u_j} = \overline{U_k U_i U_j} - \overline{U}_k\overline{U}_i\overline{U}_j - \\ - \overline{U}_k\overline{u_i u_j} - \overline{U}_i\overline{u_k u_j} - \overline{U}_j\overline{u_k u_i},\end{aligned} \tag{4.11}$$

where the first part of (4.4) has to be applied on the right-hand side.

Equation (4.10) can be used to obtain an algebraic model for the SGS stress tensor $\overline{u_i u_j}$, which is needed to close the velocity LES equation (4.3b). For that, it is convenient to split the SGS stress tensor $\overline{u_i u_j}$ into the anisotropic residual stress tensor

$$\tau_{ij} = \overline{u_i u_j} - \frac{2}{3}k_r\delta_{ij} \tag{4.12}$$

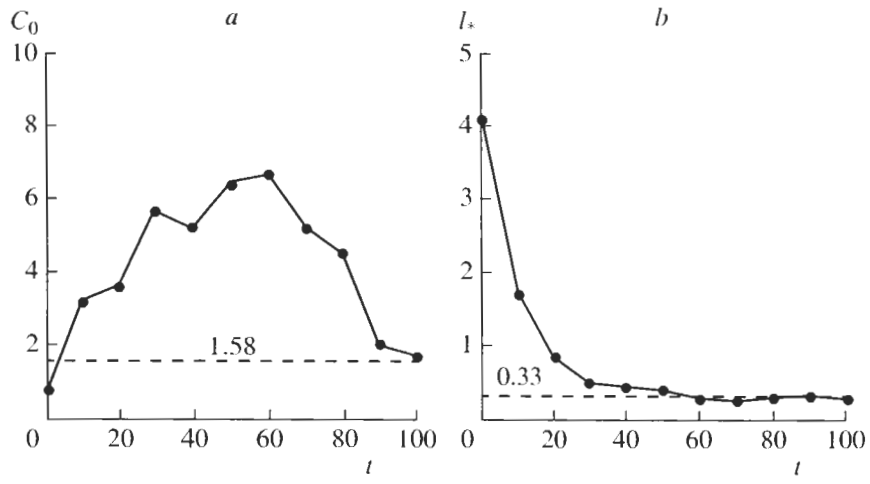

Fig. 7. The calculation of C_0 and l_* (as functions of the normalized time t) by means of the DNS data reported by Gicquel *et al.* [40]. The values $C_0 = 19/12$ and $l_* = 0.33$ obtained by theoretical arguments are shown for a comparison.

and its isotropic part $2k_r/3\delta_{ij}$, which is determined by the residual kinetic energy $k_r = \overline{u_i u_i}/2$. By restricting the attention to an incompressible flow, the analysis of (4.10) then provides in the first order of approximation the following expression for τ_{ij} [45]

$$\tau_{ij}^{(1)} = -2\nu_r \bar{S}_{ij}. \tag{4.13}$$

The residual eddy viscosity is given by $\nu_r = k_r\tau_t/3$. By adopting $\tau_L = l_*\Delta/k_r^{1/2}$ and

$$k_r = \frac{1 + 1.5C_0}{6} l_*^2 \Delta^2 |\bar{S}|^2, \tag{4.14}$$

the residual eddy viscosity ν_r is found to be $\nu_r = c_S\Delta^2|\bar{S}|$. In these relations, $|\bar{S}| = \sqrt{2\bar{S}_{kl}\bar{S}_{lk}}$ and Δ is the filter width. l_* is a number which is assumed to be non-negative. The Smagorinsky coefficient c_S is then given by [45]

$$c_S = \left(\frac{1 + 1.5C_0}{54}\right)^{1/2} l_*^2. \tag{4.15}$$

Nonlinear corrections to the linear expression (4.13) may be found in higher-order approximations. In particular, the analysis of the second-order approximation implies [45],

$$C_0 = \frac{19}{12}. \tag{4.16}$$

This value has to be seen as the asymptotic value of C_0 regarding the simulation of high-Reynolds number turbulence by means of FDF methods. It is of interest to note that the result $C_0 \approx 1.58$ obtained here agrees well with corresponding values used for C_0 within the frame of PDF methods. One often applies C_0 values in between 1 and 3 to simulate inhomogeneous and anisotropic flows at high-Reynolds numbers [2]. With regard to l_* one cannot derive a fixed value as for C_0. Instead, one finds a range of possible l_* variations [45],

$$l_* = \frac{1}{3}\left(1 \pm \frac{1}{2}\right). \tag{4.17}$$

One way to prove the suitability of these estimates for C_0 and l_* is to have a look at the implications for the Smagorinsky constant c_S. The use of (4.16) and (4.17) in (4.15) implies $c_S^{1/2} = 0.17 \pm 0.08$, which agrees well with values applied usually [1]. The calculation of c_S provided here enables also the assessment of the relation between C_0 and the Kolmogorov constant C_K that determines the energy spectrum. According to (4.17) we set $l_* = 2(8/19)^{3/4}/\pi$ in (4.15) and adopt Lilly's classical result $c_S^{1/2} = \pi^{-1}[2/(3C_K)]^{3/4}$ [46]. This leads to the relation

$$C_K = \frac{19}{12}\left(\frac{27}{8 + 12C_0}\right)^{1/3}. \tag{4.18}$$

By adopting (4.16), we find that the bracket factor in (4.18) is unity. This implies that C_0 and C_K are equal, $C_K = C_0 = 19/12 \approx 1.58$. This result for C_K agrees very well with results of measurements, which provide $C_K = (55/18)(0.53 \pm 0.055) = 1.62 \pm 0.17$ [47].

Next, we compare (4.16) and (4.17) for C_0 and l_* with available DNS data. This can be done by means of the results of Gicquel *et al.* [40]. In their notation, C_0 and l_* are given by $C_0 = 2(\tilde{C}_1 - 1)/3$ and $l_* = 2/(\tilde{C}_1\tilde{C}_\varepsilon)$. The values obtained for these parameters are presented in Fig. 7. The C_0 curve reveals two different stages. For $t < 50$, the flow evolves from an initially smooth laminar state to a three-dimensional turbulent state be-

fore the action of the small scales becomes significant [40]. Values of C_0 around 6 at $t \approx 50$ are consistent with experience obtained within the frame of PDF methods for flows of low complexity as stationary homogeneous isotropic turbulence [2]. For $t > 50$, the typical flow structures of the mixing layer considered develop [40]. C_0 approaches asymptotically to $C_0 = 19/12$, this means the theoretical finding (4.16) is well supported by these DNS results. The l_* curve is approximately constant for $t > 50$ and found in a very good agreement with the theoretical estimate $l_* = 1/3$. It is worth emphasizing that these a priori DNS calculations of C_0 and l_* are well supported by corresponding a posteriori results of Gicquel *et al.* [40], where the effects of C_0 and l_* variations on flow simulations were investigated. These findings reveal that the use of values near $C_0 = 2.1$ and $l_* = 0.5$ results in satisfactory predictions [40]. In particular, it was found that l_* should not be taken larger than $l_* = 0.5$, which agrees very well with the implications of (4.17).

4.4. The scalar FDF equation

In the framework of a model that provides only filtered velocities $\overline{U}_i$ and not instantaneous velocities, (4.9) is not the appropriate FDF equation. Rather one has to reduce (4.9) to a closed equation for the scalar FDF $F_\varphi(\boldsymbol{\theta}, \mathbf{x}, t) = \overline{\delta(\boldsymbol{\Phi}(\mathbf{x}, t) - \boldsymbol{\theta})}$. The transport equation for F_φ can be obtained by integrating (4.9) over the velocity space. This results in

$$\frac{\partial}{\partial t}\langle\rho\rangle F_\varphi = -\frac{\partial}{\partial x_i}\langle\rho\rangle(\overline{U}_i + \overline{u_i|\boldsymbol{\theta}})F_\varphi - \\ -\frac{\partial}{\partial \theta_\alpha}\langle\rho\rangle\left[\overline{\Omega}_\alpha - \frac{1}{\tau_\varphi}(\theta_\alpha - \overline{\Phi}_\alpha) + G_{\alpha m}\overline{u_m|\boldsymbol{\theta}} + S_\alpha\right]F_\varphi. \tag{4.19}$$

The closure of Eq. (4.19) requires the determination of the scalar-conditioned convective flux

$$\overline{u_i|\boldsymbol{\theta}} = F_\varphi^{-1}\overline{U_i\delta(\boldsymbol{\Phi} - \boldsymbol{\theta})} - \overline{U}_i, \tag{4.20}$$

which is defined by the right-hand side. The calculation of this quantity on the basis of the underlying velocity-scalar FDF transport equation results in

$$\overline{u_i|\boldsymbol{\theta}}F_\varphi = -K_{ik}\frac{\partial F_\varphi}{\partial x_k} \tag{4.21}$$

if counter-gradient terms are neglected [45]. The diffusion coefficient K_{ij} in (4.21) is given through

$$K_{ij} = \tau_L\gamma_{in}^{-1}\overline{u_n u_j}, \tag{4.22}$$

where γ^{-1} is the inverse matrix of γ which has elements $\gamma_{ij} = \delta_{ij} + \tau_L\partial\overline{U}_i/\partial x_j$. By neglecting shear contributions, we find in the lowest order of approximation $K_{ij} = 2\tau_L k_t/3\delta_{ij} = \nu_t/\mathrm{Sc}_t\delta_{ij}$, where the turbulence Schmidt number $\mathrm{Sc}_t = 1/2$. This theoretical value for Sc_t agrees very well with values $\mathrm{Sc}_t = 0.55 \pm 0.15$ applied in scalar FDF methods [37].

The use of (4.21) in (4.19) results in the following scalar FDF equation

$$\frac{\partial}{\partial t}\langle\rho\rangle F_\varphi = -\frac{\partial}{\partial x_i}\langle\rho\rangle\left\{\overline{U}_i F_\varphi - K_{im}\frac{\partial F_\varphi}{\partial x_m}\right\} - \\ -\frac{\partial}{\partial \theta_\alpha}\langle\rho\rangle\left\{\left[\overline{\Omega}_\alpha - \frac{1}{\tau_\varphi}(\theta_\alpha - \overline{\Phi}_\alpha) + S_\alpha\right]F_\varphi - G_{\alpha n}K_{nm}\frac{\partial F_\varphi}{\partial x_m}\right\}. \tag{4.23}$$

$G_{\alpha m}$ is given by (4.7), and the parameterization of the mixing frequency τ_φ^{-1} will be addressed in section 4.5. The solution of (4.23) permits to calculate the scalar transport in consistency with the transport equations for filtered scalars,

$$\frac{\partial\overline{\Phi}_\alpha}{\partial t} + \overline{U}_k\frac{\partial\overline{\Phi}_\alpha}{\partial x_k} = \\ = \langle\rho\rangle^{-1}\frac{\partial}{\partial x_k}\langle\rho\rangle(\nu_{(\alpha)}\delta_{km} + K_{km})\frac{\partial\overline{\Phi}_\alpha}{\partial x_m} + \bar{S}_\alpha, \tag{4.24}$$

which follow from (4.23) through multiplication with θ_α and integration over the scalar space. The extension of (4.24) through (4.23) is a requirement to involve the effects of source rates S_α on $\overline{\Phi}_\alpha$ without further approximations. A simpler approach than the use of (4.23) to obtain the scalar FDF F_φ is the assumed-shape approach where an analytical F_φ is provided to calculate $\bar{S}_\alpha$ in (4.24) via

$$\bar{S}_\alpha = \int d\boldsymbol{\theta} S_\alpha(\boldsymbol{\theta})F_\varphi(\boldsymbol{\theta}, \mathbf{x}, t). \tag{4.25}$$

Usually, one assumes that F_φ only depends on $\overline{\Phi}_\alpha$ and the scalar variances, $\overline{\phi_\alpha\phi_\beta}$. The $\overline{\Phi}_\alpha$ are then calculated according to (4.24), and the scalar variances are parameterized [48] or calculated by their transport equation. This approach is simple and relatively effective, but its range of applicability is limited. One can show that the assumption of an assumed shape for F_φ is justified if there are no velocity-scalar correlations, *i.e.*, no production mechanism for scalar fluctuations [45]. This assumption cannot be considered to be justified in general. Further, it is worth noting that the application of this approach requires the specification of the shape of the FDF F_φ. This poses a non-trivial problem: one has to provide a FDF-shape that covers both the initial and final stage of the FDF evolution. For these reasons, the solution of (4.23) represents a much more flexible method compared to the assumed-shape FDF approach.

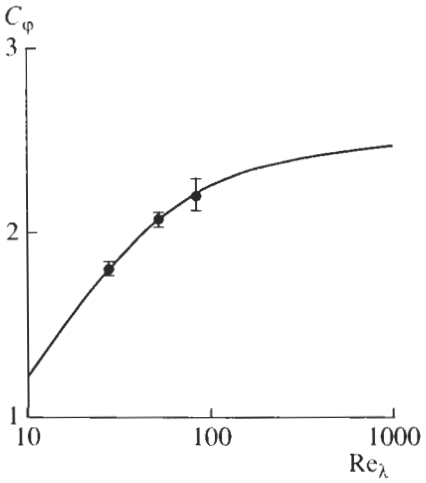

Fig. 8. The calculation of C_φ in dependence on Re_λ according to the DNS data of Overholt and Pope [51]. The error bars denote the accuracy of these data. The solid curve gives the prediction of the parameterization (4.31) combined with $C_\varphi(\infty) = 2.5$.

4.5. The scalar mixing frequency

The remaining problem is the parameterization of the mixing frequency τ_φ^{-1} in (4.23). In consistency with (4.14), the variance $\overline{\phi^2}$ of a passive scalar is found to be given by [45]

$$\overline{\phi^2} = \frac{2}{3} l_{\varphi*}^2 \Delta^2 \frac{\partial \overline{\Phi}}{\partial x_m} \frac{\partial \overline{\Phi}}{\partial x_m}. \tag{4.26}$$

Here, the parameter $l_{\varphi*}$ is introduced by $l_{\varphi*}^2 = l_*^2 (1 + \tau_\varphi/\tau_L)$. Relation (4.26) is often used to provide the scalar SGS variance within the context of assumed-shape methods [48–50]. Parameter $l_{\varphi*}$ is then calculated dynamically [48] or taken to be $l_{\varphi*} = 0.5$ [49].

The definition of $l_{\varphi*}^2$ can be used to obtain the following expression for the mixing frequency,

$$\frac{1}{\tau_\varphi} = \frac{l_*^2}{l_{\varphi*}^2 - l_*^2} \frac{1}{\tau_L}. \tag{4.27}$$

The dependence of τ_φ^{-1} on l_* corresponds to the expectation: the intensity of scalar mixing grows with the characteristic eddy length l_*. $l_{\varphi*}$ is a characteristic measure for the length over which the scalar field changes. Relation (4.27) provides for it the constraint $l_{\varphi*} > l_*$. This means that the characteristic length of the scalar field has to be larger than the characteristic eddy length, which is required for the onset of scalar mixing (scalar fields that are smaller than eddies flow with them but are not dispersed). It is worth noting that the condition $l_{\varphi*} > l_*$ is implied by the appearance of $G_{\omega m}$ in (4.5c), which provides additional support for its consideration. Equation (4.27) shows that the mixing frequency τ_φ^{-1} becomes smaller with growing $l_{\varphi*}$. This is the expected trend because τ_φ^{-1} has to vanish for $l_{\varphi*} \gg l_*$. These explanations indicate that the variability of $l_{\varphi*}$ is at least so high as that of l_*. This is confirmed by the findings of Colucci *et al.* [36] and Jaberi *et al.* [37], which reveal the need to apply different values for the constants used to parameterize τ_φ^{-1} for various flows.

By adopting the relation between τ_L and the dissipation time scale $\tau = k_r/\varepsilon_r$ of turbulence,

$$\frac{1}{\tau_L} = \frac{1 + 1.5C_0}{2\tau}, \tag{4.28}$$

which follows from the definition of $\varepsilon_r = 2k_r/[(1 + 1.5C_0)\tau_L]$, we may rewrite (4.27) into the form of the standard model for parameterizations of the scalar mixing frequency τ_φ^{-1} [1],

$$\frac{1}{\tau_\varphi} = \frac{C_\varphi}{2\tau}, \tag{4.29}$$

where C_φ is a constant that is given according to (4.27) by

$$C_\varphi = (1 + 1.5C_0) \frac{l_*^2}{l_{\varphi*}^2 - l_*^2}. \tag{4.30}$$

This result reveals that C_φ cannot be considered to be flow-independent because $l_{\varphi*}$ has to be expected to vary with the scalar field considered. Consequently, the consideration of scalar fields with significantly different characteristic length scales results in the requirement to apply different values for C_φ.

The results of DNS calculations of C_φ are given in Fig. 8, which presents the findings of Overholt and Pope's [51] investigations of passive scalar mixing in homogeneous isotropic stationary turbulence with imposed constant mean scalar gradient. The data presented are the temporal average values of C_φ obtained for the stationary portion of each simulation. The C_φ value at the Taylor-scale Reynolds number $\mathrm{Re}_\lambda = 185$ was not considered because it is strongly influenced by the forcing energy input [51]. The solid curve in Fig. 8 represents a parameterization of the dependence of C_φ on Re_λ,

$$C_\varphi = \frac{C_\varphi(\infty)}{1 + 1.7 C_\varphi^2(\infty) \mathrm{Re}_\lambda^{-1}}. \tag{4.31}$$

The structure of this formula is chosen according to the corresponding parameterization of C_0 suggested by Sawford [52]. Further support for such a variation of C_φ with Re_λ is provided by recent results of Heinz and Roekaerts [53]. The parameters in (4.31) were estimated such that the predictions of (4.31) agree with the DNS

data. This leads to the asymptotic value $C_\varphi(\infty) = 2.5$ of C_φ. The use of this value (combined with $C_0 = 19/12$ and $l_* = 1/3$) in (4.30) implies then $l_{\varphi*} = 0.5$, which agrees with the assumption of Forkel and Janicka [49].

5. SUMMARY

With regard to the development of optimal RANS models (the first problem considered in the introduction), one may draw the following conclusions. Such models can be developed by a stepwise reduction of DNS data, as shown in section 2 for wall-bounded compressible flows. The turbulence model parameters are obtained in this way as functions that vary in space. With regard to the turbulence Prandtl numbers Sc_t, Pr_t, Pr_k and Pr_ω in the mass fraction, temperature, turbulent kinetic energy and frequency equation, respectively, the variations of DNS data appear to be hardly relevant such that the use of effective values $Sc_t = Pr_t = Pr_k = Pr_\omega = 0.9$ is well justified. However, the same is not the case for other parameters, as C_μ and S_ω. For them, one needs non-trivial parameterizations which are non-universal, as may be seen by the inapplicability of standard modeling assumptions that were proved to be appropriate for the modeling of other turbulent flows.

With regard to the improvement of micromixing models (the second problem considered in the introduction), we observe the following. An improved stochastic model for the transport of scalars can be constructed on the basis of a projection method. The predictions of this model agree very well with DNS data of scalar mixing in stationary, homogeneous and isotropic turbulence obtained by Juneja and Pope [26]. However, this model performance requires the inclusion of memory effects and noise that it confined by a bound model. The latter model features were found to be important, in particular, with regard to the first stage of mixing which is relevant to non-premixed combustion problems (the asymptotic stage of mixing may be well simulated by the simpler model (3.10)). Therefore, in correspondence to the features of RANS velocity models for wall-bounded compressible flows one needs relatively complex and (in general) flow-dependent models in order to obtain accurate simulation results.

As an alternative to the use of PDF (and implied RANS) methods, one can limit model assumptions to the simulation of small-scale processes. This leads to the questions of which stochastic equations are appropriate for the modeling of small-scale turbulence (the third question considered in the introduction). As shown in section 4, such stochastic models have a much simpler and relatively universal structure (with regard to the scalar model, for example, there is no need to involve memory effects, external noise and a bound model). Adjustments to different flows may be performed by varying the model parameters l_* and $l_{\varphi*}$ (which can be also calculated by means of dynamic procedures) [45]. The obvious disadvantage of this approach is related to the fact that the solution of such equations is much more expensive than the use of corresponding PDF or RANS methods. Therefore, the combination of the accuracy of FDF (LES) methods with the efficiency of PDF (RANS) methods seems to be an optimal way – but the development of such unified turbulence models requires solutions for a couple of relevant questions [2].

REFERENCES

1. *Pope S.B.* Turbulent Flows. Cambridge: Cambridge University Press, 2000.
2. *Heinz S.* Statistical Mechanics of Turbulent Flows. N.Y.: Springer-Verlag, 2003.
3. *Fox R.O.* Computational Models for Turbulent Reacting Flows, Cambridge Series in Chemical Engineering. Cambridge: Cambridge University Press, 2003.
4. *Foysi H., Friedrich R.* // Proc. 3rd Intern. Sympos. on Turbulence and Shear Flow Phenomena, Sendai, Japan, 2003. P. 1121.
5. *Foysi H., Sarkar S., Friedrich R.* // Proc. 3rd Intern. Sympos. on Turbulence and Shear Flow Phenomena. Sendai, Japan. 2003. P. 1103.
6. *Foysi H., Sarkar S., Friedrich R.* // J. Fluid Mech. 2004. V. 509. P. 207.
7. *Sesterhenn J.* // Computers & Fluids. 2001. V. 30. P. 37.
8. *Adams N.A., Shariff K.* // J. Comp. Phys. 1996. V. 127. P. 27.
9. *Lele S.* // J. Comp. Phys. 1992. V. 103. P. 16.
10. *Williamson J.H.* // J. Comp. Phys. 1980. V. 35. P. 48.
11. *Lechner R.* Sesterhenn J., Friedrich R. // J. Turbulence. 2001. V. 2. P. 1.
12. *Moser R.D., Kim J., Mansour N.N.* // Phys. Fluids. 1999. V. 11. P. 943.
13. *Wilcox D.C.* Turbulence Modeling for CFD. Second edition. DCW Industries, Inc., 1998.
14. *Heinz S., Foysi H., Friedrich R.* // Turbulent supersonic channel flow: Statistical modeling based on direct numerical simulation data. 2005 (submitted).
15. *Pope S.B.* // Prog. Energy Combust. Sci. 1985. V. 11. P. 119.
16. *Fox R.O.* // Phys. Fluids. 1992. V. 4. P. 1230.
17. *Valino L., Dopazo C.* // Phys. Fluids. 1991. V. 3. P. 3034.
18. *Grabert H.* Projection Operator Technique in Nonequilibrium Statistical Mechanics. Berlin, Heidelberg, New York, Tokyo: Springer-Verlag, 1982.
19. *Lindenberg K., West J.W.* The Nonequilibrium Statistical Mechanics of Open and Closed System. New York, Weinheim, Cambridge VHC Publishers, Inc. 1990.
20. *Zubarev D., Morozov V., Röpke G.* Statistical Mechanics of Nonequilibrium Processes. Basic Concepts, Kinetic Theory. Berlin: Akademie Verlag (VCH Publishers), 1996. V. 1.
21. *Zubarev D., Morozov V., Röpke G.* Statistical Mechanics of Nonequilibrium Processes. Relaxation and Hydrodynamic Processes. Berlin: Akademie Verlag (VCH Publishers), 1997. V. 2.
22. *Heinz S.* // Phys. Fluids. 1997. V. 9. P. 703.
23. *Fox R.O.* // Phys. Fluids. 1994. V. 6. P. 334.

24. *Gardiner C.W.* Handbook of Statistical Methods. Berlin, Heidelberg, New York, Tokyo: Springer-Verlag, 1983.
25. *Risken H.* The Fokker-Planck Equation. Berlin, Heidelberg, New York: Springer-Verlag, 1984.
26. *Juneja A., Pope S.B.* // Phys. Fluids. 1996. V. 8. P. 2161.
27. *Eswaran V., Pope S.B.* // Phys. Fluids. 1988. V. 31. P. 506.
28. *Heinz S.* // Flow, Turb. Combust. 2003. V. 70. P. 115.
29. *Menevau C., Katz J.* // Annu. Rev. Fluid Mech. 2000. V. 32. P. 1.
30. *Piomelli U.* // Prog. Aerosp. Sci. 1999. V. 35. P. 335.
31. *Sagaut P.* Large Eddy Simulation for Incompressible Flows. New York: Springer-Verlag, 2001.
32. *Givi P.* // Prog. Energy Combust. Sci. 1989. V. 15. P. 1.
33. *Madnia C.K., Givi P.* // Large Eddy Simulations of Complex Engineering and Geophysical Flows / Eds. Galperin B., Orszag S.A. Cambridge: Cambridge University Press, 1993. P. 315.
34. *Pope S.B.* // Proc. 23rd Sympos. (Intern.) on Combust. Pittsburg: The Combus. Institute, 1990. P. 591.
35. *Gao F., O'Brien E.E.* // Phys. Fluids. 1993. V. 5. P. 1282.
36. *Colucci P.J., Jaberi F.A., Givi P., Pope S.B.* // Phys. Fluids. 1998. V. 10. P. 499.
37. *Jaberi F.A., Colucci P.J., James S., Givi P., Pope S.B.* // J. Fluid Mech. 1999. V. 401. P. 85.
38. *Reveillon J., Vervisch L.* // AIAA J. 1998. V. 36. P. 336.
39. *Zhou X.Y., Pereira J.C.F.* // Flow, Turb. Combust. 2000. V. 64. P. 279.
40. *Gicquel L.Y. M., Givi P., Jaberi F.A., Pope S.B.* // Phys. Fluids. 2002. V. 14. P. 1196.
41. *Muradoglu M., Jenny P., Pope S.B., Caughey D.A.* // J. Comput. Phys. 1999. V. 154. P. 342.
42. *Nooren P.A., Wouters H.A., Peeters T.W.J., Roekaerts D.* // Combust. Theory and Modeling. 1997. V. 1. P. 79.
43. *Wouters H.A., Nooren P.A., Peeters T.W.J., Roekaerts D.* // Proc. 26th Sympos. (Intern.) on Combust. Pittsburgh: The Combust. Institute, 1996. P. 177.
44. *Vreman B., Geurts B., Kuerten H.* // J. Fluid Mech. 1994. V. 278. P. 351.
45. *Heinz S.* // Flow, Turb. Combust. 2003. V. 70. P. 153.
46. *Lilly D.K.* // Proc. IBM Scientific Computing Sympos. on Environmental Sciences. Ed. Goldstine H.H. N.Y.: Yorktown Heights, 1967. P. 195.
47. *Sreenivasan K.R.* // Phys. Fluids. 1995. V. 7. P. 2778.
48. *Wall C., Boersma B.J., Moin P.* // Phys. Fluids. 2000. V. 12. P. 2522.
49. *Forkel H., Janicka J.* // Flow, Turb. Combust. 2000. V. 65. P. 163.
50. *Pierce C., Moin P.* // Phys. Fluids. 1998. V. 10. P. 3041.
51. *Overholt M.R., Pope S.B.* // Phys. Fluids. 1996. V. 8. P. 3128.
52. *Sawford B.L.* // Phys. Fluids. 1991. V. 3. P. 1577.
53. *Heinz S., Roekaerts D.* // Chem. Eng. Sci. 2001. V. 56. P. 3197.